Journal of Zhejiang University SCIENCE A
ISSN 1673-565X (Print); ISSN 1862-1775 (Online)
www.zju.edu.cn/jzus; www.springerlink.com
E-mail: jzus@zju.edu.cn

Numerical study of PV/T-SAHP system*

Gang PEI, Jie JI†‡, Ke-liang LIU, Han-feng HE, Ai-guo JIANG

(*Department of Thermal Science and Energy Engineering, University of Science and Technology of China, Hefei 230027, China*)

†E-mail: jijie@ustc.edu.cn

Received Dec. 24, 2007; revision accepted Feb. 27, 2008

Abstract: In order to utilize solar energy effectively and to achieve a higher electrical efficiency by limiting the operating temperature of the photovoltaic (PV) panel, a novel photovoltaic/thermal solar-assisted heat pump (PV/T-SAHP) system was proposed and constructed. The hybrid solar system generates electricity and thermal energy simultaneously. A distributed parameters model of the PV/T-SAHP system was developed and applied to analyze the system dynamic performance in terms of PV action, photothermal action and Rankine cycle processes. The simulation results indicated that the coefficient of performance (COP) of the proposed PV/T-SAHP can be much better than that of the conventional heat pump. Both PV-efficiency and photothermic efficiency have been improved considerably. The results also showed that the performance of this PV/T-SAHP system was strongly influenced by the evaporator area, tube pitch and tilt angle of the PV/T evaporator, which are the key factors in PV/T-SAHP system optimization and PV/T evaporator design.

Key words: Photovoltaic (PV), Photothermic, Heat pump, Photovoltaic/thermal (PV/T) evaporator
doi:10.1631/jzus.A0720143 **Document code:** A **CLC number:** TK01

INTRODUCTION

Due to the depletion nature of fossil fuels, the use of alternative energy sources, like solar energy, is receiving wider attention for heating, cooling and power generation applications. Theoretically, the maximum possible efficiency of a single crystalline silicon solar cell is about 25% under global AM1.5 spectrum (1000 W/m^2) at 25 °C. However, the maximum efficiency drops rapidly to 14% at 100 °C (Ristinen and Kraushaar, 1999; Green *et al*., 2006). This loss of efficiency is mainly due to the drop in open-circuit cell voltage. Theoretical studies showed that such a loss is inevitable, so it is needed to effectively cool the solar cells for achieving good photovoltaic (PV) (Wysocki and Rappaport, 1960; Sze, 1981). Moreover, other losses, such as edge loss and back loss, make the efficiency of a commercial standard PV panel lower which only ranges from 10% to 14%. Most of the solar energy striking on a PV panel is converted into heat energy. How to utilize this waste heat to support space heating, water heating, or other household activities has been a current subject of interest—a research area known as the photovoltaic/thermal (PV/T) technology which is to convert solar radiation into electricity and thermal energy simultaneously. Another reason for the hybrid option is the importance of cooling the solar cells. In some cases, this is achieved by means of an air stream—a technique mainly applying in building integrated PV/T systems, where warm air is used for space heating purpose (Cox and Raghuraman, 1985; Sopian and Yigit, 1996).

In order to achieve more effective cooling, water is used to replace air as the heat-transfer medium (Kamoshida *et al.*, 1991). Imre *et al.*(1993) presented such a PV/T design concept with the module either glazed or unglazed, which can be integrated into the building structure. Fujisawa and Tani (1997) introduced similar PV/T systems with single glass cover, and showed that the thermal zero loss efficiency of

‡ Corresponding author

* Project supported by the National Natural Science Foundation of China (No. 50708105), and partly supported by the Natural Science Foundation of Anhui Province (No. 070414161), China

the system could be above 0.7. Vries (1998) carried out a detailed study of water-type PV/T collectors, through both theoretical and experimental works.

In most water-type PV/T systems, the coolant flow conduits are integrated directly with the PV module. For household applications, the required temperature of the service water should be at least 50 °C, which means the PV operating temperature would be higher than 50 °C so that the PV-efficiency drops considerably. This mismatch between water temperature and PV-efficiency has restricted the development of PV/T systems (Garg and Agarwal, 1995; Ji *et al*., 2003a; Chow, 2003).

On the other hand, the global concerns about energy saving have made the use of heat pumps increasing popular for residential, commercial and industrial applications. With the lengthy application, the heat pumps have undergone many significant design changes that make them much reliable and competitive compared with other heating equipments designed for conventional fuels such as oil. Solar-assisted heat pump (SAHP), a special kind of heat pump, has been studied for several years. An SAHP is composed of a Rankine-refrigeration-cycle unit that is coupled with a solar collector as the evaporator. It has been demonstrated that a high coefficient of performance (COP) can be achieved through the system due to heat pump and solar energy of their complimentary characteristics (Chaturvedi and Shen, 1984; Morrison, 1994; Hawlader *et al*., 2001; Kuang *et al*., 2003). A heat pump operates more efficiently at higher evaporating temperature whereas a PV module operates more efficiently at lower temperatures. The PV module and the heat pump evaporator can be favorably integrated as a single component, known as the PV/T evaporator. Fig.1 shows its design features, as constructed in our system. During operation, a portion of the solar radiation on the PV/T evaporator is converted to electricity through the PV cells, and the major part goes to thermal energy. The latter serves as a heat source for refrigerant evaporation—a process that lowers more considerably the operating temperature of the PV/T evaporator than in a conventional PV module. On the other hand, because of the direct insulation, its evaporating temperature is higher than that in a normal heat pump. As a result, by integrating PV action, photothermic action together with the Rankine cycle, the PV-efficiency, photothermic efficiency and COP of the heat pump are overall improved in the hybrid PV/T-SAHP design.

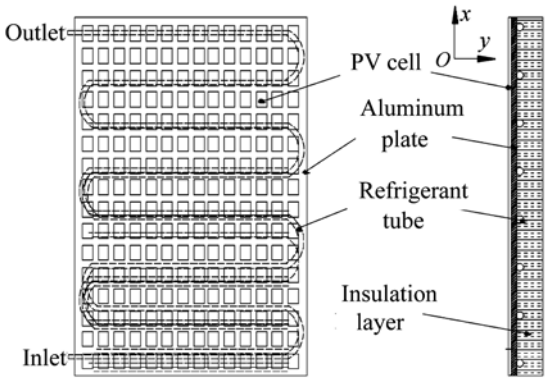

Fig.1 Schematic diagram of PV/T evaporator

Ito *et al.*(1997; 2005) carried out experiments in Japan to study the effect of bonding the PV modules onto the flat-plate evaporator of an SAHP. It was concluded that the PV modules on the evaporator had negligible effects on the performance of the SAHP, and a high level of COP had been reached. The experiments by Ito *et al.*(1997; 2005) were primarily focused on the thermal performance. In our study, as presented below, the PV performance of PV module, the general PV/T application of solar radiation, and the performance of heat pump were all evaluated systematically. A dynamic distributed parameters model was developed to analyze the thermal, PV and general PV/T performance of the PV/T-SAHP system.

Fig.2 shows a brief schematic diagram of our proposed PV/T-SAHP system. The convective evaporator, connected in parallel with the PV/T evaporator, only works on cloudy days to replace the duty of the PV/T evaporator. The water bath condenser provides warm water for space heating and other household applications. The convective condenser can directly provide warm air for space heating in winter. The operating mode of the PV/T-SAHP system is governed by the valve positions. With a four-way valve at the compressor outlet (not shown in Fig.2), the system can provide space cooling in summer on top of its heating functions, and thus extended its service as a multi-functional PV/T-SAHP system.

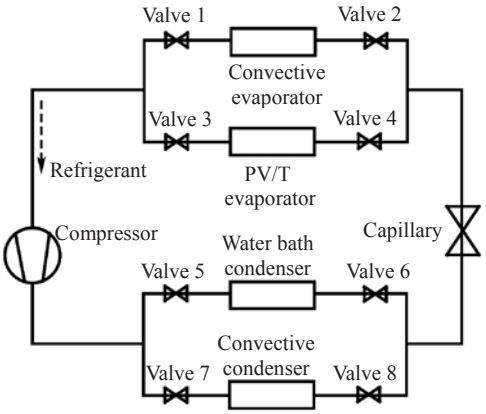

Fig.2 Schematic diagram of PV/T-SAHP system

MATHEMATICAL MODEL

The PV/T-SAHP system model mainly includes two parts: a PV/T evaporator model and a heat pump Rankine cycle model. This model was developed to simulate the system dynamic performance, primarily under the daily variation of meteorological data. How the system characteristics are influenced by the design parameters (like evaporator area, tilt angle, tube pitch, and so on) can also be analyzed.

PV/T evaporator model

The PV/T evaporator consists of PV cells, heat-carrying aluminum plate, refrigerant tubes, thermal insulation layer and aluminum frame. The configuration is showed in Fig.1. The PV cells are affixed to the topside of the aluminum plate; the refrigerant tubes are welded to its back surface and covered by the thermal insulation layer. Thermal energy is to conduct well all the way through the PV cells, the aluminum plate and the refrigerant tube.

For the PV/T evaporator plate (including the aluminum plate and the PV cells), let ρ, δ and C be respectively the density (kg/m^3), thickness (m) and specific heat capacity (J/(kg·K)) of the plate, then

$$\rho\delta C\frac{\mathrm{d}T}{\mathrm{d}t}=I\alpha-E+(h_\mathrm{c}+h_\mathrm{r})(T_\mathrm{a}-T)+hA_\mathrm{ref}(T_\mathrm{ref}-T)+(T_\mathrm{a}-T)/R_\mathrm{in}, \tag{1}$$

where T_a is the temperature of ambient air, K; T_ref the temperature of refrigerant, K; T the temperature of the plate, K; I the instantaneous solar irradiance falling on the evaporator, W/m^2; α the effective absorptivity of plate; E the electric power output of the PV cells, W; h_c the convective heat transfer coefficients of air, W/(m^2·K); h_r the radiation heat transfer coefficients, W/(m^2·K); h the convective heat transfer coefficient of refrigerant flow in tube; A_ref the inner surface area of the flow channels per unit surface area of the plate, m^2; R_in the thermal resistance between plate and the ambient air at the back of the PV/T evaporator, (m^2·K)/W.

Fig.3 shows one portion of the PV/T evaporator between two adjacent refrigeration tube sections. The pitch of two parallel tube sections is defined as the tube pitch L_0 (m). If the heat conduction in the y direction (the tube running direction) can be neglected, the heat-transfer behavior of the PV/T evaporator through thermal conduction can be described as:

$$\begin{cases}\dfrac{\partial T}{\partial t}=\dfrac{k}{\rho C}\dfrac{\partial^2 T}{\partial x^2}+[U_\mathrm{l}(T_\mathrm{a}-T)+I(\tau\alpha)],\\ k\left(\dfrac{\partial T}{\partial X}\right)_{x=L_0/2}=0,\\ k\left(\dfrac{\partial T}{\partial X}\right)_{x=0}=\dfrac{\pi Dh}{2\delta}(T_\mathrm{r}-T_\mathrm{p}),\\ T_{\tau=0}=T_\mathrm{a},\end{cases} \tag{2}$$

where k is the thermal conductivity of the PV/T evaporator, W/(m·K); $(\tau\alpha)$ the product of transmissivity and absorptivity; D the inner diameter of the refrigerant tube, m; δ the wall thickness of the refrigerant tube, m; x the distance of a point at the aluminum plate from the nearest tube position, m.

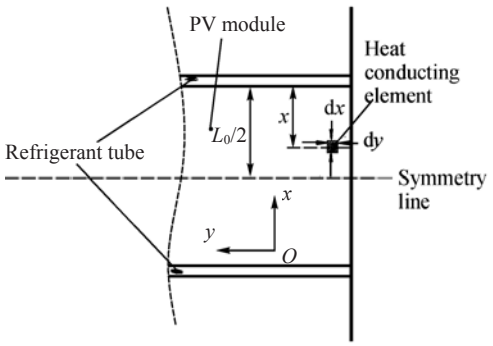

Fig.3 Part diagram of PV/T evaporator

For an unglazed PV/T evaporator, the overall heat loss coefficient U_l (W/(m^2·K)) has a significant

effect on the collector performance. Two components are involved: back loss and top loss, i.e.,

$$U_l = U_t + U_b, \tag{3}$$

where the back loss coefficient U_b (W/(m^2·K)) is usually negligible when the evaporator is properly insulated; the top loss coefficient U_t (W/(m^2·K)) is a function of the radiation and convective heat loss coefficients.

For such a forced boundary layer flow, the convective heat loss coefficient h_c can be written as (Kreith, 1973)

$$h_c = 0.036(Pr)^{0.33} k_a (Re_L^{0.80} - 23200.0)/L, \tag{4}$$

where Pr is the Prandtl number of air; k_a the thermal conductivity of air, W/(m·K); Re_L the Reynolds number based on evaporator length; L the width of PV/T evaporator, m. The wind direction was assumed parallel to the surface of the PV modules.

The radiation heat loss coefficient can be written as (Duffie and Beckman, 1980)

$$h_r = \varepsilon \frac{\sigma(T^4 - T_{sky}^4)}{T - T_a}, \tag{5}$$

and

$$T_{sky} = 0.0552 T_a^{1.5}, \tag{6}$$

where T_{sky} is the sky temperature, K; σ the Stephan-Boltzman constant, W/(m^2·K^4); β the tilt angle of the evaporator, °.

The pressure drop inside the refrigerant tube is determined by treating the two-phase mixture as homogeneous and then applying the mass, momentum and energy balances. The equation, after simplification, is expressed as (Chaturvedi *et al*., 1982):

$$-\frac{dp}{dz} = \frac{\dfrac{2C_f G^2}{D}[v_f + x v_g] + G^2 v_{fg} \dfrac{dx}{dz}}{\left\{1 + G^2 \left[x \dfrac{dv_g}{dp} + (1-x) \dfrac{dv_f}{dp} \right]\right\}}, \tag{7}$$

where G is the mass flux of refrigerant, kg/(m^2·s); x the dryness fraction which varies with the evaporating pressure and specific enthalpy of the wet vapor; v_f and v_g are the specific volumes (m^3/kg) of saturated liquid and saturated vapor, respectively and are the functions of evaporating pressure only. The friction coefficient, C_f, is a function of the tube Reynolds number, and its functional form depends on whether the flow is laminar or turbulent (Chaturvedi *et al*., 1982):

$$C_f = 0.079 / Re_{D_i}^{0.25}, \quad \text{for laminar flow,} \tag{8a}$$

$$C_f = 16 / Re_{D_i}, \quad \text{for turbulent flow,} \tag{8b}$$

where D_i is the equivalent diameter.

Since x=x(p,h), we can write the following expression

$$\frac{dx}{dz} = \left(\frac{\partial x}{\partial p}\right)_h \frac{dp}{dz} + \left(\frac{\partial x}{\partial h}\right)_p \frac{dh}{dz} = \frac{1}{h_{fg}} \frac{dh}{dz} + \left(\frac{\partial x}{\partial p}\right)_h \frac{dp}{dz}. \tag{9}$$

In the absence of large pressure drops, $\left(\dfrac{\partial x}{\partial p}\right)_h \dfrac{dp}{dz} << \dfrac{1}{h_{fg}} \dfrac{dh}{dz}$, so Eq.(9) can be simplified as

$$\frac{dx}{dz} = \frac{1}{h_{fg}} \frac{dh}{dz}. \tag{10}$$

Through the aluminum plate and the circulation tube, heat energy is transferred from the PV cells to the refrigerant (R-22). The heat transfer coefficient between the tube and the refrigerant can be given by the Dittus-Boelter correlation for single-phase flows (Shah, 1979), i.e.,

$$Nu = 0.023 Re^{0.8} Pr^{0.3}, \tag{11}$$

where

$$Nu = hD/k, \qquad Re = GD/\mu, \tag{12}$$

and for two-phase flows,

$$h_{tp} = h\left[(1-x)^{0.8} + \frac{3.8x^{0.76}(1-x)^{0.04}}{Pr^{0.38}}\right]. \tag{13}$$

The electric power output E of the PV modules is correlated to the working temperature (Ji *et al*., 2003a), in that

$$E=\frac{I\left[a+b(T_{\mathrm{p}}-298.15)\right]}{I_{\mathrm{e}}A_{\mathrm{e}}}, \tag{14}$$

where the calibration radiation I_e is 970 W/m^2; calibration area A_e is 0.485 m^2; a is 66.42 W and b is –0.244 W/K.

The overall efficiency of the PV/T evaporator is defined as

$$\overline{\eta}=\overline{\eta}_{\mathrm{t}}+\overline{\eta}_{\mathrm{e}}, \tag{15}$$

where $\overline{\eta}_t$ and $\overline{\eta}_e$ are the photothermic efficiency and the PV-efficiency of the PV/T evaporator, respectively. They are the time-averaged values given by

$$\overline{\eta}_{\mathrm{t}}=\frac{\int_{\tau_1}^{\tau_2}\dot{m}_{\mathrm{act}}(h_{\mathrm{out}}-h_{\mathrm{in}})\mathrm{d}\tau}{A_{\mathrm{c}}\int_{\tau_1}^{\tau_2}I\mathrm{d}\tau}, \tag{16}$$

and

$$\overline{\eta}_{\mathrm{e}}=\frac{\int_{\tau_1}^{\tau_2}E\mathrm{d}\tau}{\int_{\tau_1}^{\tau_2}I\mathrm{d}\tau}, \tag{17}$$

where A_c is the radiation receiving area of the PV/T evaporator, m^2; h_{in} and h_{out} are the specific enthalpies of the refrigerant at the PV/T evaporator inlet and outlet, kJ/kg.

Heat pump system model

A portion of the solar radiation received by the PV/T evaporator is converted into electricity, while most of the other portion is converted into thermal energy. Heat pump upgrades the absorbed thermal energy to a higher temperature level, and discharges the energy in the condenser. On the other hand, in the evaporator tube the refrigerant fully vaporizes and cools the PV modules. This improves the overall efficiency of the PV/T-SAHP system.

The thermodynamic cycle of the heat pump is shown on a *T*-*S* diagram in Fig.4. Sub-cooled refrigerant, flowing out of the condenser (at Point 7), is first throttled in the capillary tube or the expansive valve (through the Process 7-8), then enters the PV/T evaporator (at Point 8). In the evaporator, the refrigerant absorbs heat from the solar irradiation and vaporizes gradually. At the evaporator output (Point 2), the refrigerant reaches the slightly superheated state, and is further acted on by the compressor and discharged as a high temperature high pressure superheated gas at the outlet end (Point 3). Then it enters the condenser where it is cooled to become a sub-cooled liquid (the Process 3-7). One heat pump thermodynamic cycle is therefore completed.

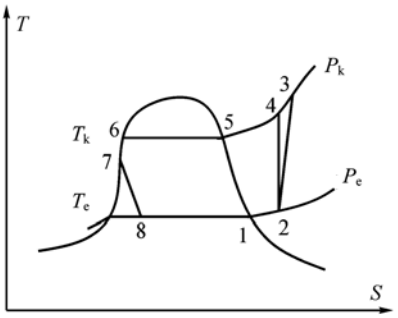

T_k: condensing temperature, °C; T_e: evaporating temperature, °C; P_k: condensing pressure, Pa; P_e: evaporating pressure, Pa

Fig.4 Thermodynamics cycle of heat pump

During the operation, the PV/T evaporator directly absorbs solar radiation as the heat source for the heat pump cycle. The evaporating temperature changes in accordance with the instantaneous meteorological conditions like solar radiation intensity; so are the changes in compressor working conditions. The complexity makes the traditional mathematical model of a heat pump compressor not suitable for PV/T-SAHP. The authors in a previous study (Ji *et al*., 2005) had developed the following heat pump compressor model, which is also suitable for the application where the evaporating temperature may fluctuate tremendously.

The actual mass flow rate $\dot{m}_{\mathrm{act}}$ and actual power N_{act} of the compressor are given (Ji *et al*., 2005) by

$$\dot{m}_{\mathrm{act}}=\dot{m}_{\mathrm{th}}F_1(T_{\mathrm{cd}},T_{\mathrm{ev}}), \tag{18}$$

and

$$N_{\mathrm{act}}=N_{\mathrm{in}}F_2(T_{\mathrm{cd}},T_{\mathrm{ev}}), \tag{19}$$

where $F_1(T_{cd},T_{ev})$ and $F_2(T_{cd},T_{ev})$ are the curve-fit functions based on the compressor experimental data. The theoretical refrigerant mass flow rate $\dot{m}_{\mathrm{th}}$ (kg/s) is given (Ji *et al*., 2005) by

$$\dot{m}_{\mathrm{th}} v_{\mathrm{suc}} = 60\lambda_{\mathrm{v}}\lambda_{\mathrm{p}}\lambda_{\mathrm{T}}\lambda_{\mathrm{D}} n\pi R^2 S\varepsilon(2-\varepsilon), \qquad (20)$$

where v_{suc} is the specific volume of refrigerant at the suction end, m^3; n the number of cylinders, R the inner radius of cylinder, m; S the stroke of the cylinder, m; and ε the eccentricity of cylinder. The subscripts 'v', 'p', 'T' and 'D' of the compressor coefficients λ respectively stand for volume, pressure, temperature and leakage effects. The theoretical compressor power input is then (Ji *et al*., 2005)

$$N_{\mathrm{th}} = \dot{V}_{\mathrm{th}}\eta_{\mathrm{v}} \frac{P_{\mathrm{ev}} m}{m-1}\left[\left(\frac{P_{\mathrm{cd}}}{P_{\mathrm{ev}}}\right)^{\frac{m-1}{m}} - 1\right], \qquad (21)$$

where $\dot{V}_{\mathrm{th}}$ is the theoretical volume flow rate, m^3/s; η_{v} the volumetric efficiency; m the index of polytropic compression; P_{ev} and P_{cd} respectively the evaporating and condensing pressures, Pa. The system power input at compressor is given by

$$N_{\mathrm{in}} = \frac{1}{\eta_{\mathrm{mo}}}\left(\frac{N_{\mathrm{th}}}{\eta_{\mathrm{i}}} + N_{\mathrm{l}}\right), \qquad (22)$$

where N_{l} is the power loss by friction; η_{i} and η_{mo} are the isentropic and motor efficiencies, respectively.

The refrigerant mass flow rate through the capillary tube can be determined by the following empirical equation (Jung and Park, 1999)

$$\dot{m} = C_1 D^{C_2} L^{C_3} T_{\mathrm{cd}}{}^{C_4} 10^{C_5 \times DSC}, \qquad (23)$$

where the coefficients C_1=0.249029, C_2=2.543633, C_3=–0.42753, C_4=0.746108 and C_5=0.013922; DSC is degree of superheat.

SYSTEM SIMULATION AND RESULT ANALYSIS

Hefei, a city located at 31.87° N and 117.23° E, is in the middle-south region of China. The weather dataset of one typical sunny day of Hefei, the 9th of May, 2005, was used in this simulation study. The data was obtained from a typical weather file on the website of 3E HV&AC developed by Tsinghua University (http://www.hvacr.com.cn/, Feb. 14, 2007). Fig.5 shows the daily variation of ambient temperature, beam radiation and diffuse radiation on that day. The average dry bulb temperature was 22.97 °C, the average beam radiation 661.68 W/m^2, the average diffuse radiation 32.38 W/m^2, and the average wind velocity 4.5 m/s.

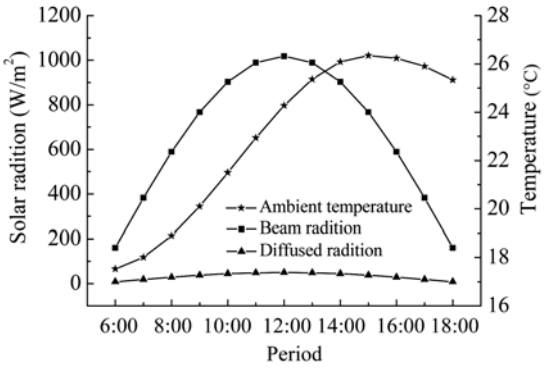

Fig.5 Meteorological data of May 9, 2005 in Hefei, China

For the PV/T evaporator, the specifications of the single-crystalline silicon solar cell which are referred to the standard testing conditions of 25 °C and 1000 W/m^2 are shown in Table 1. Other PV/T-SAHP parameters used in the computation are in Table 2.

Table 1 Specifications of the solar cell

Parameter	Value
Net cell area on PV/T evaporator (cm^2)	156.25
Photovoltaic efficiency (%)	15.4
Open circuit voltage (V)	0.627
Close circuit current (A)	5.115
Maximum power (W)	2.402
Voltage at the maximum point (V)	0.529
Current at the maximum point (A)	4.583

Table 2 PV/T- SAHP parameters

Parameter	Value
Input power of compressor (W)	1200
Diameter of refrigerant tube (mm)	6
Thermal conductivity of aluminum plate (W/(m·K))	237
Thermal conductivity of refrigerant tube (W/(m·K))	401
Emissivity at PV-module	0.90
Absorptivity at PV-module	0.85
Condenser water temperature at inlet (°C)	20
Condenser water temperature at outlet (°C)	50

The thermal properties of the refrigerant R-22 were determined by the equations listed in Table 3.

In order to analyze the performance of this PV/T-SAHP system influenced by: (i) the evaporator area A_c, (ii) the tilt angle β, and (iii) the tube pitch L_0, a range of these three variables were evaluated in the simulation. The value of A_c were set to 6 m^2, 9 m^2, 12 m^2 and 15 m^2 (i.e., at 3 m^2 intervals); β from 0° to 90°, at 10° intervals; L_0 from 0.1 to 0.5 m, at 0.1 m intervals. The simulation results are shown in Figs.6~15. In the following discussions, the values of A_c, β and L_0 are made reference to the case of 9 m^2, 30°, and 0.2 m, respectively, unless they are specified otherwise.

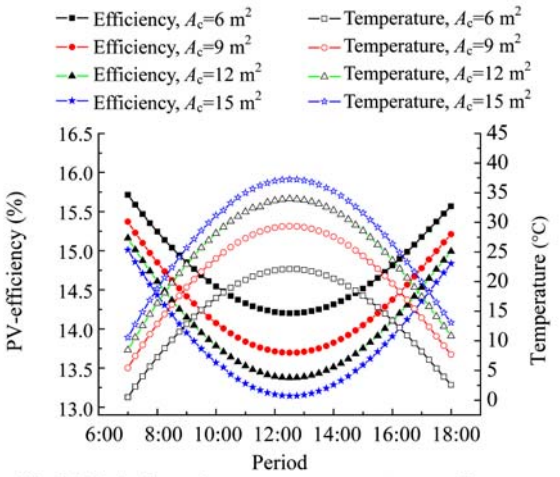

Fig.6 Variation of average temperature and average PV-efficiency with time

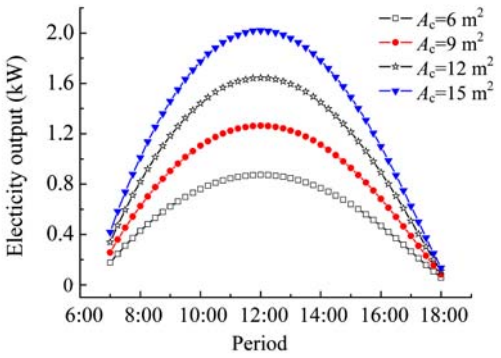

Fig.7 Variation of electrical power output with time

PV/T efficiency

The simulation results are given in Figs.6 and 7. The graphs show that the electricity output of the PV/T evaporator increases with the increase of the solar beam radiation, but the PV-efficiency declines on the contrary. In the early morning, PV-efficiency starts with a peak at 15.4%. At noon it reduces to 13.7%, and in the afternoon it gradually increases again, giving a daily average value of 14.3%. The electricity output has its peak at 1.1 kW, and the daily average value is about 0.864 kW.

Table 3 Thermal properties of the refrigerant R-22

Thermal property	Calculation equation
Specific heat of constant volume	$c_{v0}=0.04135T_r^4-0.21960T_r^3+0.29043T_r^2+0.31010T_r+0.20428$
Pressure of supersaturated vapor	$p=10RT_cT_r\rho\left[1+\sum_{i=1}^{9}\left(\sum_{j=0}^{3}b_{ij}/T_r^j\right)\rho^i\right]$
Enthalpy of supersaturated vapor	$h=-\int\left[T_r\left(\frac{\partial p}{\partial T_r}\right)_\rho-p\right]\rho^{-2}\mathrm{d}\rho+\frac{p}{\rho}+\int c_{v0}\mathrm{d}T+492.348$
Entropy of supersaturated vapor	$s=-T_c^{-1}\int\left(\frac{\partial p}{\partial T_r}\right)\rho^{-2}\mathrm{d}\rho+\int\frac{c_{v0}}{T}\mathrm{d}T+4.1745$
Enthalpy of saturated liquid	$h'=h''-0.1T_rT_c(1/\rho''-1/\rho')\frac{\mathrm{d}p_s}{\mathrm{d}T}$
Entropy of saturated liquid	$s'=s''-0.1(1/\rho''-1/\rho')\frac{\mathrm{d}p_s}{\mathrm{d}T}$
Density of saturated liquid	$\rho'=\rho_c\exp\{a_1(1-T_r)^{1/3}+a_2(T_r-1)[0.2(T_r+1)^2+0.5]\}$
Enthalpy of wet vapor	$h_x=xh''+(1-x)h'$
Entropy of wet vapor	$s_x=xs''+(1-x)s'$
Pressure of saturated vapor	$p_s=p_c\exp[Ri\ln T_r+(Ri-4+P_\alpha)\varphi(T_r)]$, where $\varphi=4[(T_r-1)/T_r]+(T_r-1)[0.2(T_r+1)^2+0.5]-5.3\ln T_r$

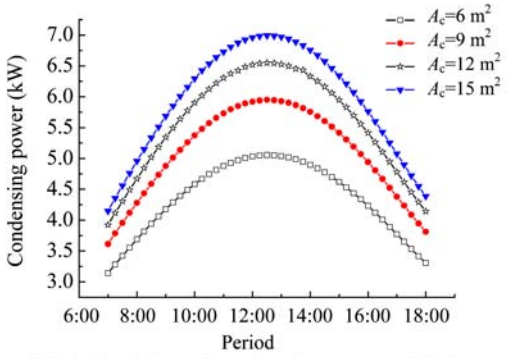

Fig.8 Variation of condensing power with time

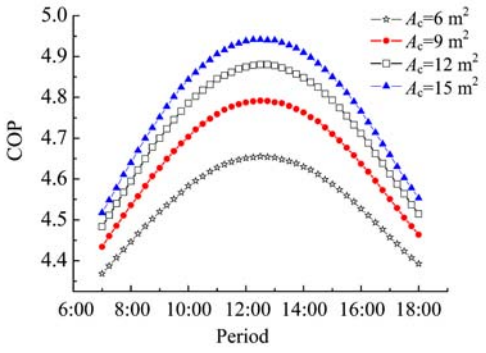

Fig.9 Variation of heat pump COP with time

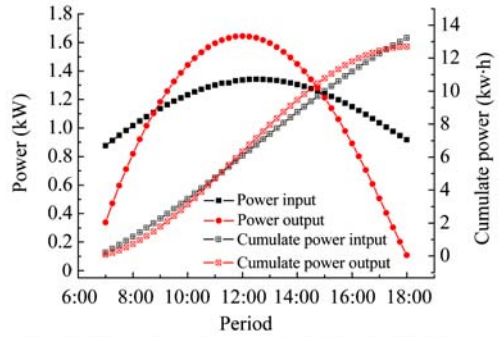

Fig.10 Variation of power in/output with time

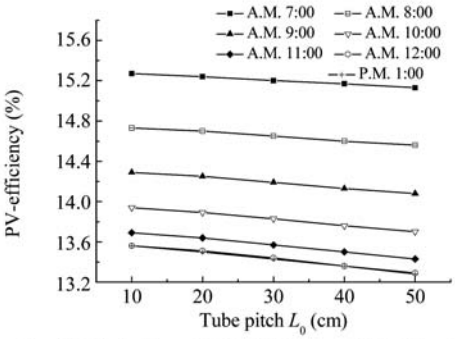

Fig.11 Variation of PV-efficiency with tube pitch

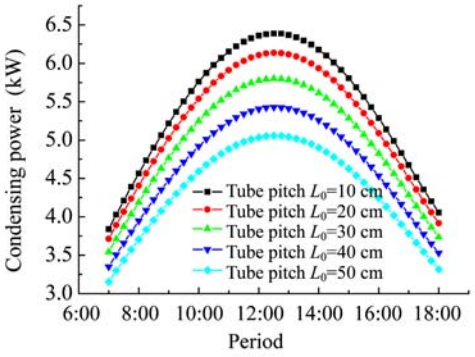

Fig.12 Variation of condensing power with time

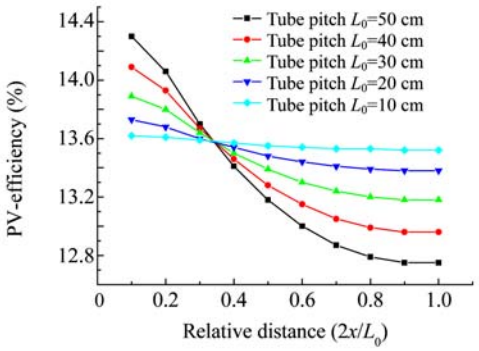

Fig.13 Variation of PV-efficiency with $2x/L_0$

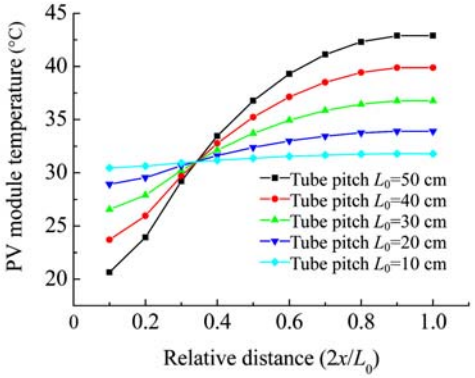

Fig.14 Variation of PV temperature with $2x/L_0$

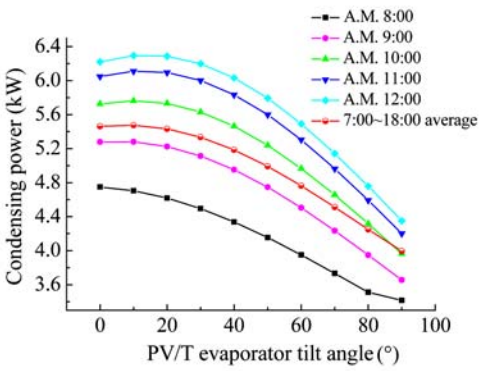

Fig.15 Variation of condensing power with tilt angle

The PV-efficiency of an ordinary PV module is only about 12.3% (Ji *et al.*, 2003a). Hence the PV-efficiency of the proposed PV/T-SAHP system is 16.3% higher. Also from the simulation results, the average photothermic efficiency was found 70.4% and the overall PV/T-efficiency added up to 84.7%. So by working with a lower temperature level, the overall energy conversion efficiency of PV/T-SAHP is much higher than that of the traditional solar devices. For example, the efficiency of the best vacuum tube system is about 60%. By comparison, the overall conversion efficiency of PV/T-SAHP is 41.2% higher.

Heat pump COP

Figs.8 and 9 show that both the condensing power and the heat pump COP increase with the increase of the solar beam radiation. At 7:00 in the morning, the condensing power is 3.5 kW, and at 12:30 it becomes 5.7 kW. This reveals that under direct sunlight, the PV/T evaporator operates at a higher evaporating temperature than the convective one does, thus contributing to a higher COP than an ordinary heat pump. On the 9th of May for instance, the PV/T-SAHP system gained 220×10^6 J heat energy throughout the day with an average COP of 4.66. Compared to the ordinary heat pump with a COP of 3.25, the increase is about 43% for very similar testing conditions in Hefei (Ji *et al*., 2003b).

Energy consumption

The energy consumption of PV/T-SAHP can be defined as the difference between its electricity input and electricity output. In Fig.10, from 8:15 to 15:00, the electricity output of the PV modules is more than the system electricity input, but the output is less than the input at the other 4 h. Within the whole day, the accumulated electricity input was 13.2 kW·h, and the accumulated electricity output was 12.7 kW·h. Taking the electricity efficiency of the converter and the storage battery as 0.75, the net energy consumption is 3.8 kW·h for the day. If the ordinary convective heat pump (with a COP of 2.7) was used to gain the same amount of heat, the consumed electricity would be 22.9 kW·h. The electricity consumed by the ordinary heat pump is therefore about five times more than that by the PV/T-SAHP system.

In actual operation, there can be a net output of electric power from PV/T-SAHP if the compressor works intermittently. For example, if the compressor works only from 10:00~14:00 of the day, the system can then not only cover its own electricity consumption, but also have a net electricity output of 6.0 kW·h.

Optimization of the PV/T evaporator

Figs.11 and 12 show that the increase of the tube pitch L_0 will lead to a distinct decrease of average PV-efficiency, as well as condensing power. When L_0 is reduced from 50 cm to 10 cm, the maximum condensing power increases by 28% from 5 kW to 6.4 kW.

Figs.13 and 14 show the variation of PV-efficiency and temperature distribution at the PV/T evaporator with the normalized distance ($2x/L_0$). When L_0 is 10 cm, the temperature of the PV module has a variation of 1.3 °C along the x direction and the PV-efficiency has a variation of 0.1%. When L_0 is 50 cm, the temperature of the PV module has a variation of 22.2 °C along the x direction and the PV-efficiency has a variation of 1.5%. Apparently, the smaller the variation in temperature, the better is the PV module operating condition.

Figs.6~10 show that, although the increase in evaporator surface area for receiving solar radiation may lead to a decrease of PV-efficiency, it improves the output power, COP, condensing power, and so on. Figs.15 and 16 show that, when the tilt angle changed from 0° to 30°, the electric power output and the condensing power of the heat pump changed very little at Hefei in May. When the tilt angle changed from 30° to 90°, however, the electric power output and the condensing power declined rapidly. Their minimum values are respectively 23% and 75% of the

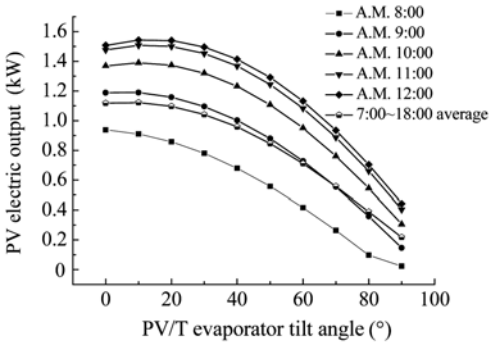

Fig.16 Variation of electrical output with tilt angle

maximums. The output electric power and the condensing power had their peak values when the tilt angle was between 0° and 15°.

CONCLUSION

The simulation shows that our novel PV/T-SAHP system greatly enhances the overall solar energy utilization and the thermal performance of the heat pump. Its PV-efficiency is 16% higher than that of the conventional PV system and its COP is about 43% higher than that of the conventional heat pump. The overall PV/T-efficiency of the PV/T-SAHP system can reach 84.7%. Considering the electrical performance, the energy consumed by the PV/T-SAHP system is only one sixth that of the conventional heat pump. Evaporator area, tilt angle and tube pitch are the key design parameters to be investigated in system optimization.

The PV/T-SAHP system proposed in this paper has a significant potential for space heating and domestic water heating in the subtropical region such as the south-middle region in China, where there is a widespread demand of fuel oil and electricity for domestic heating. The PV/T-SAHP system works favorably compared with the ordinary heat pump and solar energy systems. More comprehensive economic analysis and operating experiences are needed to determine the practicality of this PV/T-SAHP system. The high PV/T-efficiency in hybrid solar technology and high COP in heat pump application indicate that an optimized version of the PV/T-SAHP may compete effectively with the conventional residential heating equipments in the near future.

References

Chaturvedi, S.K., Shen, J.Y., 1984. Thermal performance of a direct expansion solar-assisted heat pump. *Solar Energy*, **33**(2):155-162. [doi:10.1016/0038-092X(84)90233-0]

Chaturvedi, S.K., Chiang, Y.F., Roberts, A.S., 1982. Analysis of two phase flow collectors with application to heat pumps. *ASME Journal of Solar Energy Engineering*, **104**(4):358-365.

Chow, T.T., 2003. Performance analysis of photovoltaic-thermal collector by explicit model. *Solar Energy*, **75**(2):143-152. [doi:10.1016/j.solener.2003.07.001]

Cox, C.H., Raghuraman, P., 1985. Design considerations for flat-plate-photovoltaic/thermal collectors. *Solar Energy*, **35**(3):227-241. [doi:10.1016/0038-092X(85)90102-1]

Duffie, J.A., Beckman, W.A., 1980. Solar Engineering of Thermal Processes. Wiley, New York, p.122-123.

Fujisawa, T., Tani, T., 1997. Binary utilization of solar energy with photovoltaic thermal hybrid collector. *Proceedings of ISES Solar World Congress*, **2**:559-564.

Garg, H.P., Agarwal, R.K., 1995. Some aspects of a PV/T collector/forced circulation flat plats solar water heater with solar cells. *Energy Conversion and Management*, **36**(2):87-99. [doi:10.1016/0196-8904(94)00046-3]

Green, M.A., Emery, K., King, D.L., Hisikawa, Y., Warta, W., 2006. Solar cell efficiency tables (version 27). *Progress in Photovoltaics Research and Applications*, **14**(1):45-51. [doi:10.1002/pip.686]

Hawlader, M.N.A., Chou, S.K., Ullah, M.Z., 2001. The performance of a solar heat pump water heating system. *Applied Thermal Engineering*, **21**(10):1049-1065. [doi:10.1016/S1359-4311(00)00105-8]

Imre, L., Bitai, A., Boehoenyer, F., 1993. PV-thermal combined building elements. *Proceedings of ISES Solar World Congress*, **3**:277-280.

Ito, S., Miura, N., Wang, J.Q., 1997. Heat pump using a solar collector with photovoltaic modules on the surface. *ASME Journal of Solar Energy Engineering*, **119**(2):147-151. [doi:10.1115/1.2887894]

Ito, S., Miura, N., Takano, Y., 2005. Studies of Heat pumps using direct expansion type solar collectors. *ASME Journal of Solar Energy Engineering*, **127**(1):60-64. [doi:10.1115/1.1824102]

Ji, J., Chow, T.T., He, W., 2003a. Dynamic performance of hybrid photovoltaic/thermal collector wall in Hong Kong. *Building and Environment*, **38**(11):1327-1334. [doi:10.1016/S0360-1323(03)00115-X]

Ji, J., Chow, T.T., Pei, G., Dong, J., He, W., 2003b. Domestic air-conditioner and integrated water heater for subtropical climate. *Applied Thermal Engineering*, **23**(5):581-592. [doi:10.1016/S1359-4311(02)00228-4]

Ji, J., Pei, G., Chowm T.T., He, W., Zhang, A.F., Dong, J., Yi, H., 2005. Performance of multi-functional domestic heat pump system. *Applied Energy*, **80**(3):307-326. [doi:10.1016/j.apenergy.2004.04.005]

Jung, D., Park, C., 1999. Capillary tube selection for HCFC22 alternatives. *International Journal of Refrigeration*, **22**(8):604-614. [doi:10.1016/S0140-7007(99)00027-4]

Kamoshida, J., Isshhiki, N., Katayama, K., 1991. Optical/thermal design and simulation of fixed line focus fresnel concentrator for combined photovoltaic-thermal applications. *Proceedings of ISES Solar World Congress*, **1**:374-378.

Kreith, F., 1973. Principle of Heat Transfer. Intex Educational Publishers. New York, p.309-382.

Kuang, Y.H., Wang, R.Z., Yu, L.Q., 2003. Experimental study on solar assisted heat pump system for heat supply. *Energy Conversion and Management*, **44**(7):1089-1098. [doi:10.1016/S0196-8904(02)00110-3]

Morrison, G.L., 1994. Simulation of packaged solar heat-pump water heaters. *Solar Energy*, **53**(3):249-257. [doi:10.1016/0038-092X(94)90631-9]

Ristinen, R.A., Kraushaar, J.J., 1999. Energy and the Environment. Wiley, New York.

Shah, M.M., 1979. A general correlation for heat transfer during film condensation inside pipes. *International Journal of Heat and Mass Transfer*, **22**(4):547-556. [doi:10.1016/0017-9310(79)90058-9]

Sopian, K., Yigit, K.S., 1996. Performance analysis of photovoltaic thermal air heaters. *Energy Conversion and Management*, **37**(11):1657-1670. [doi:10.1016/0196-8904(96)00010-6]

Sze, S.M., 1981. Physics of Semiconductor Devices. Willey, New York, p.790-839.

Vries, D.W., 1998. Design of a Photovoltaic/thermal Combi-panel. Eindhoven University Press, Eindhoven, p.1-112.

Wysocki, J.J., Rappaport, P., 1960. Effect of temperature on photovoltaic solar energy conversion. *Journal of Applied Physics*, **31**:571-577. [doi:10.1063/1.1735630]